New Journal of Physics
The open access journal for physics

Precision measurement of the B_s^0–$\overline{B}_s^0$ oscillation frequency with the decay $B_s^0 \to D_s^- \pi^+$

The LHCb Collaboration

New Journal of Physics **15** (2013) 053021 (15pp)
Received 18 April 2013
Published 14 May 2013
Online at http://www.njp.org/
doi:10.1088/1367-2630/15/5/053021
E-mail: wandernoth@physi.uni-heidelberg.de

Abstract. A key ingredient to searches for physics beyond the Standard Model in B_s^0 mixing phenomena is the measurement of the B_s^0–$\overline{B}_s^0$ oscillation frequency, which is equivalent to the mass difference Δm_s of the B_s^0 mass eigenstates. Using the world's largest B_s^0 meson sample accumulated in a dataset, corresponding to an integrated luminosity of $1.0\,\text{fb}^{-1}$, collected by the LHCb experiment at the CERN LHC in 2011, a measurement of Δm_s is presented. A total of about 34 000 $B_s^0 \to D_s^- \pi^+$ signal decays are reconstructed, with an average decay time resolution of 44 fs. The oscillation frequency is measured to be $\Delta m_s = 17.768 \pm 0.023\,(\text{stat}) \pm 0.006\,(\text{syst})\,\text{ps}^{-1}$, which is the most precise measurement to date.

Contents

1. Introduction

The Standard Model (SM) of particle physics, despite its great success in describing experimental data, is considered an effective theory valid only at low energies, below the TeV scale. At higher energies, new physics phenomena are predicted to emerge. For analyses looking for physics beyond the SM (BSM), there are two conceptually different approaches: direct and indirect searches. Direct searches are performed at the highest available energies and aim at producing and detecting new heavy particles. Indirect searches focus on precision measurements of quantum-loop-induced processes. Accurate theoretical predictions are available for the heavy quark sector in the SM. It is therefore an excellent place to search for new phenomena [1, 2], since any deviation from these predictions can be attributed to contributions from BSM.

In the SM, transitions between quark families (flavours) are possible via the charged current weak interaction. Flavour changing neutral currents (FCNC) are forbidden at lowest order, but are allowed in higher order processes. Since new particles can contribute to these loop diagrams, such processes are highly sensitive to contributions from BSM. An example FCNC transition is neutral meson mixing, where neutral mesons can transform into their antiparticles. Particle–antiparticle oscillations have been observed in the K^0–$\overline{K}^0$ system [3], the B^0–$\overline{B}^0$ system [4], the B_s^0–$\overline{B}_s^0$ system [5, 6] and the D^0–$\overline{D}^0$ system [7–10]. The frequency of B_s^0– $\overline{B}_s^0$ oscillations is the highest. On average, a B_s^0 meson changes its flavour nine times between production and decay. This poses a challenge to the detector for the measurement of the decay time. Another key ingredient of this measurement is the determination of the flavour of the B_s^0 meson at production, which relies heavily on good particle identification and the separation of tracks from the primary interaction point.

The observed particle and antiparticle states B_s^0 and $\overline{B}_s^0$ are linear combinations of the mass eigenstates B_H and B_L with masses m_H and m_L and decay widths Γ_H and Γ_L, respectively [11]. The B_s^0 oscillation frequency is equivalent to the mass difference $\Delta m_s = m_H - m_L$. The parameter Δm_s is an essential ingredient for all studies of time-dependent matter–antimatter

asymmetries involving B_s^0 mesons, such as the B_s^0 mixing phase ϕ_s in the decay $B_s^0 \to J/\psi\phi$ [12]. It was first observed by the Collider Detector at Fermilab (CDF) [6]. The Large Hadron Collider beauty experiment (LHCb) published a measurement of this frequency using a dataset, corresponding to an integrated luminosity of $37\,\text{pb}^{-1}$, taken in 2010 [13]. This analysis complements the previous result and is obtained in a similar way, using a data sample, corresponding to an integrated luminosity of $1.0\,\text{fb}^{-1}$, collected by LHCb in 2011.

2. The LHCb experiment

The LHCb experiment is designed for precision measurements in the beauty and charm hadron systems. At a centre-of-mass energy of $\sqrt{s} = 7\,\text{TeV}$, about 3×10^{11} $b\bar{b}$ pairs were produced in 2011. The LHCb detector [14] is a single-arm forward spectrometer covering the pseudorapidity range from two to five. The excellent decay time resolution necessary to resolve the fast B_s^0–$\overline{B}_s^0$ oscillation is provided by a silicon-strip vertex detector surrounding the pp interaction region. At nominal position, the sensitive region of the vertex detector is only 8 mm away from the beam. An impact parameter (IP) resolution of 20 μm for tracks with high transverse momentum (p_T) is achieved.

Charged particle momenta are measured with the LHCb tracking system consisting of the aforementioned vertex detector, a large-area silicon-strip detector located upstream of a dipole magnet with a bending power of about 4 T m, and three stations of silicon-strip detectors and straw drift tubes placed downstream. The combined tracking system has momentum resolution $\Delta p/p$ that varies from 0.4% at $5\,\text{GeV}/c$ to 0.6% at $100\,\text{GeV}/c$.

Since this analysis is performed with decays involving only hadrons in the final state, excellent particle identification is crucial to suppress background. Charged hadrons are identified using two ring-imaging Cherenkov detectors [15]. Photon, electron and hadron candidates are identified by a calorimeter system consisting of scintillating-pad and preshower detectors, an electromagnetic calorimeter and a hadronic calorimeter. Muons are identified by a system composed of alternating layers of iron and multiwire proportional chambers.

The first stage of the trigger [16] is implemented in hardware, based on information from the calorimeter and muon systems, and selects events that contain candidates with large transverse energy and transverse momentum. This is followed by a software stage that applies a full event reconstruction. The software trigger used in this analysis requires a two-, three- or four-track secondary vertex with a significant displacement from the primary interaction, a large sum of p_T of the tracks, and at least one track with $p_T > 1.7\,\text{GeV}/c$. In addition, an IP χ^2 with respect to the primary interaction greater than 16 and a track fit χ^2 per degree of freedom <2 is required. The IP χ^2 is defined as the difference between the χ^2 of the primary vertex reconstructed with and without the considered track. A multivariate algorithm is used for the identification of the secondary vertices.

For the simulation, pp collisions are generated using PYTHIA 6.4 [17] with a specific LHCb configuration [18]. Decays of hadronic particles are described by EVTGEN [19], in which final state radiation is generated using PHOTOS [20]. The interaction of the generated particles with the detector and its response are implemented using the GEANT4 toolkit [21, 22], as described in [23].

3. Signal selection and analysis strategy

The analysis uses B_s^0 candidates reconstructed in the flavour-specific decay mode[1] $B_s^0 \to D_s^- \pi^+$ in five D_s^- decay modes, namely $D_s^- \to \phi(K^+K^-)\pi^-$, $D_s^- \to K^{*0}(K^+\pi^-)K^-$, $D_s^- \to K^+K^-\pi^-$ nonresonant, $D_s^- \to K^-\pi^+\pi^-$ and $D_s^- \to \pi^-\pi^+\pi^-$. To avoid double counting, events that contain a candidate passing the selection criteria of one mode are not considered for the subsequent modes, using the order listed above. All reconstructed decays are flavour-specific final states; thus the flavour of the B_s^0 candidate at the time of its decay is given by the charges of the final state particles. A combination of tagging algorithms is used to identify the B_s^0 flavour at production. The algorithms provide for each candidate a tagging decision as well as an estimate of the probability that this decision is wrong (mistag probability). These algorithms have been optimized using large event samples of flavour-specific decays [24, 25].

To be able to study the effect of selection criteria that influence the decay time spectrum, we restrict the analysis to those events in which the signal candidate passed the requirements of the software trigger algorithm used in this analysis. Specific features, such as the masses of the intermediate ϕ and K^{*0} resonances or the Dalitz structure of the $D_s^- \to \pi^-\pi^+\pi^-$ decay mode, are exploited for the five decay modes. The most powerful quantity to separate signal from background common to all decay modes is the output of a boosted decision tree (BDT) [26]. The BDT exploits the long B_s^0 lifetime by using as input the IP χ^2 of the daughter tracks, the angle of the reconstructed B_s^0 momentum relative to the line between the reconstructed primary vertex, and the B_s^0 vertex and the radial flight distance in the transverse plane of both the B_s^0 and the D_s^- mesons. Additional requirements are applied on the sum of the p_T of the B_s^0 candidate's decay products as well as on particle identification variables, and on track and vertex quality. The reconstructed D_s^- mass is required to be consistent with the known value [27]. After this selection, a total of about 47 800 candidates remain in the $B_s^0 \to D_s^- \pi^+$ invariant mass window of 5.32–5.98 GeV/c^2.

An unbinned likelihood method is employed to simultaneously fit the B_s^0 invariant mass and decay time distributions of the five decay modes. The probability density functions (PDFs) for signal and background in each of the five modes can be written as

$$\mathcal{P} = \mathcal{P}_m(m)\,\mathcal{P}_t(t, q|\sigma_t, \eta)\,\mathcal{P}_{\sigma_t}(\sigma_t)\,\mathcal{P}_\eta(\eta), \tag{1}$$

where m is the reconstructed invariant mass of the B_s^0 candidate, t is its reconstructed decay time and σ_t is an event-by-event estimate of the decay time resolution. The tagging decision q can be 0 if no tag is found, -1 for events with different flavour at production and decay (mixed) or +1 for events with the same flavour at production and decay (unmixed). The predicted event-by-event mistag probability η can take values between 0 and 0.5. The functions $\mathcal{P}_m$ and $\mathcal{P}_t$ describe the invariant mass and the decay time probability distributions, respectively. $\mathcal{P}_t$ is a conditional probability depending on σ_t and η. The functions $\mathcal{P}_{\sigma_t}$ and $\mathcal{P}_\eta$ are required to ensure the proper relative normalization of $\mathcal{P}_t$ for signal and background [28]. The functions $\mathcal{P}_{\sigma_t}$ and $\mathcal{P}_\eta$ are determined from data, using the measured distribution in the upper B_s^0 invariant mass sideband for the background PDF and the sideband subtracted distribution in the invariant mass signal region for the signal PDF.

This measurement has been performed 'blinded', meaning that during the analysis process the fitted value of Δm_s was shifted by an unknown value, which was removed after the analysis procedure had been finalized.

[1] Unless explicitly stated, inclusion of charge-conjugated modes is implied.

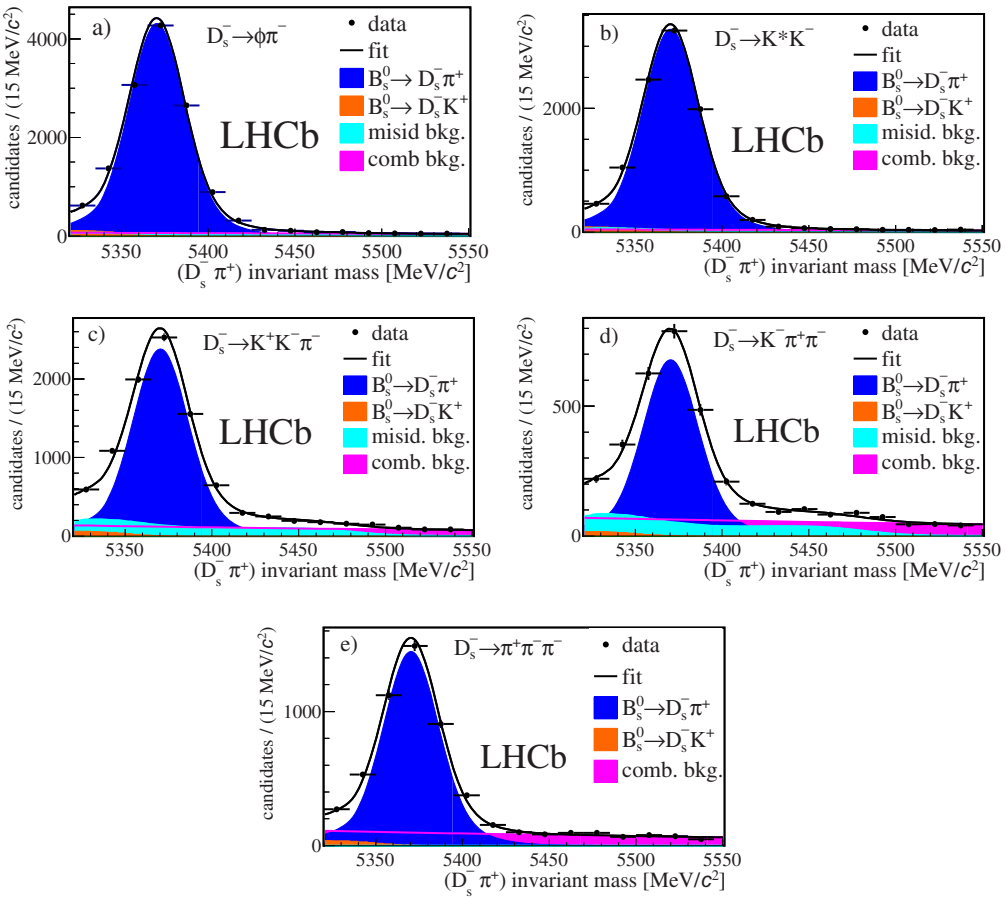

Figure 1. Invariant mass distributions for $B_s^0 \to D_s^-\pi^+$ candidates with the D_s^- meson decaying as (a) $D_s^- \to \phi(K^+K^-)\pi^-$, (b) $D_s^- \to K^{*0}(K^+\pi^-)K^-$, (c) $D_s^- \to K^+K^-\pi^-$ nonresonant, (d) $D_s^- \to K^-\pi^+\pi^-$ and (e) $D_s^- \to \pi^-\pi^+\pi^-$. The fits and the various background components are described in the text. Misidentified backgrounds refer to background from B^0 and Λ_b^0 decays with one misidentified daughter particle.

4. Invariant mass description

The invariant mass of each B_s^0 candidate is determined in a vertex fit constraining the D_s^- invariant mass to its known value [27]. The invariant mass spectra for the five decay modes after all the selection criteria are applied are shown in figure 1. The fit to the five distributions takes into account contributions from signal, combinatorial background and b-hadron decay backgrounds. The signal components are described by the sum of two Crystal Ball (CB) functions [29], which are constrained to have the same peak parameter. The parameters of the CB function describing the tails are fixed to values obtained from simulation, whereas the mean and the two widths are allowed to vary. These are constrained to be the same for all five decay modes. It has been checked on data that the mass resolution is compatible among all modes.

The b-hadron decay background includes B^0 and Λ_b^0 decays with one misidentified daughter particle. Their mass shapes are derived from simulated samples. The yields for the

Table 1. Number of candidates and B_s^0 signal fractions in the mass range 5.32–5.98 GeV/c^2.

Decay mode	$(D_s^-\pi^+)$ candidates	$f_{B_s^0\to D_s^-\pi^+}$	$f_{B_s^0\to D_s^\mp K^\pm}$
$D_s^-\to\phi(K^+K^-)\pi^-$	14 691	0.834 ± 0.008	
$D_s^-\to K^{*0}(K^+\pi^-)K^-$	10 866	0.857 ± 0.009	
$D_s^-\to K^+K^-\pi^-$ nonresonant	11 262	0.595 ± 0.009	
$D_s^-\to K^-\pi^+\pi^-$	4288	0.437 ± 0.014	
$D_s^-\to\pi^-\pi^+\pi^-$	6674	0.599 ± 0.008	0.019 ± 0.010
Total	47 781	0.714 ± 0.004	0.019 ± 0.010

different b-hadron decay backgrounds are allowed to vary individually for each of the five decay modes. Another component originates from $B_s^0\to D_s^\mp K^\pm$ decays, in which the kaon is misidentified as a pion. This contribution is treated as a signal in the decay time analysis.

The requirement that the invariant mass be larger than 5.32 GeV/c^2 rejects background candidates from B_s^0 decays with additional particles in the decay not reconstructed, such as $B_s^0\to D_s^{*-}\pi^+(D_s^{*-}\to D_s^-\pi^0$ or $D_s^-\gamma)$. The fitted number of signal candidates does not change with respect to a fit in a larger mass window. The high mass sideband region 5.55–5.98 GeV/c^2 provides a sample of mainly combinatorial background candidates. The mass distribution is described by an exponential function, whose parameters are allowed to vary individually for the five decay modes. By including this region in the fit, we are able to determine the decay time distribution as well as the tagging behaviour of the combinatorial background.

The number of used candidates along with the signal fractions extracted from the two-dimensional fit in mass and decay time are reported in table 1. One complication arises from the fact that the shape of the invariant mass distribution of the $B_s^0\to D_s^\mp K^\pm$ events is very similar to that of the B^0 background. Therefore, the fraction of $B_s^0\to D_s^\mp K^\pm$ candidates has been determined in a fit to the $D_s^-\to\pi^-\pi^+\pi^-$ mode only, in which no B^0 background is present. Subsequently this value is used for all the other modes.

5. Decay time description

The decay time of a particle is measured as

$$t=\frac{Lm}{p}, \tag{2}$$

where L is the distance between the production vertex and the decay vertex of the particle, m its reconstructed invariant mass and p its reconstructed momentum. We use the decay time calculated without the D_s^- mass constraint to avoid a systematic dependence of the B_s^0 decay time on the reconstructed invariant mass. The theoretical distribution of the decay time, t, ignoring the oscillation and any detector resolution, is

$$\mathcal{P}_t\propto\Gamma_s\,e^{-\Gamma_s t}\,\cosh\left(\frac{\Delta\Gamma_s}{2}t\right)\theta(t), \tag{3}$$

where Γ_s is the B_s^0 decay width and $\Delta\Gamma_s$ the decay width difference between the light and heavy mass eigenstates[2]. The value for $\Delta\Gamma_s$ is fixed to the latest value measured by LHCb [12] $\Delta\Gamma_s = 0.106 \pm 0.011 \pm 0.007\,\text{ps}^{-1}$. It is varied within its uncertainties to assess the systematic effect on the measurement of Δm_s. The Heaviside step function $\theta(t)$ restricts the PDF to positive decay times.

To account for detector resolution effects, the decay time PDF is convolved with a Gaussian distribution. The width σ_t is taken from an event-by-event estimate returned by the fitting algorithm that reconstructs the B_s^0 decay vertex. Due to tracking detector resolution effects, σ_t needs to be calibrated. A data-driven method, combining prompt D_s^- mesons from the primary interaction with random π^+ mesons, forms fake B_s^0 candidates. The decay time distribution of these candidates, each divided by its event-by-event σ_t, is fitted with a Gaussian function. The width provides a scale factor $S_{\sigma_t} = 1.37$, by which each σ_t is multiplied, such that it represents the correct resolution. By inspecting different regions of phase space of the fake B_s^0 candidates, the uncertainty range on this number is found to be $1.25 < S_{\sigma_t} < 1.45$. The variation is taken into account as part of the Δm_s systematic studies. The resulting average decay time resolution is $S_{\sigma_t} \times \langle\sigma_t\rangle = 44\,\text{fs}$.

Some of the selection criteria influence the shape of the decay time distribution, e.g. the requirement of a large IP for B_s^0 daughter tracks. Thus, a decay time acceptance function $\mathcal{E}_t(t)$ has to be taken into account. Its parametrization is determined from simulated data and the parameter describing its shape is allowed to vary in the fit to the data, while Γ_s is fixed to the nominal value [27]. Taking into account resolution and decay time acceptance, the PDF given in equation (3) is modified to

$$\mathcal{P}_t(t|\sigma_t) \propto \left[\Gamma_s\, e^{-\Gamma_s t}\, \cosh\left(\frac{\Delta\Gamma_s}{2}t\right)\, \theta(t)\right] \otimes G(t; 0, S_{\sigma_t}\sigma_t)\mathcal{E}_t(t) \tag{4}$$

with $G(t; 0, S_{\sigma_t}\sigma_t)$ being the resolution function determined by the method mentioned above. The decay time PDFs for the B^0 and Λ_b^0 backgrounds are identical to the signal PDF, except for $\Delta\Gamma$ being zero, and Γ_s being replaced by their respective decay widths [27]. The shape of the decay time distribution of the combinatorial background is determined with high mass sideband data. It is parametrized by the sum of two exponential functions multiplied by a second-order polynomial distribution. The exponential and polynomial parameters are allowed to vary in the fit and are constrained to be the same for the five decay modes.

6. Flavour tagging

To determine the flavour of the B_s^0 meson at production, both opposite-side (OST) and same-side (SST) tagging algorithms are used. The OST exploits the fact that b quarks at the LHC are predominantly produced in quark–antiquark pairs. By partially reconstructing the second b hadron in the event, conclusions on the flavour at production of the signal B_s^0 candidate can be drawn. The OST has been optimized on large samples of $B^+ \to J/\psi K^+$, $B \to \mu^+ D^{*-} X$ and $B^0 \to D^-\pi^+$ decays [24].

The SST takes advantage of the fact that the net strangeness of the pp collision is zero. Therefore, the s quark needed for the hadronization of the B_s^0 meson must have been produced in association with an $\bar{s}$ quark, which in about 50% of the cases hadronizes to form a charged kaon.

[2] $\Delta\Gamma_s$ and Δm_s are measured in units with $\hbar = 1$ throughout this paper.

By identifying this kaon, the flavour at production of the signal B_s^0 candidate is determined. The optimization of the SST was performed on a data sample of $B_s^0 \to D_s^- \pi^+$ decays, which has a large overlap with the sample used in this analysis [25]. However, since the oscillation frequency is not correlated with the parameters describing tagging performance, this does not bias the Δm_s measurement.

The decisions given by both tagging algorithms have a probability ω to be incorrect. Each tagging algorithm provides an estimate for the mistag probability η; which is the output of a neural network combining various event properties. The true mistag probability ω can be parametrized as a linear function of the estimate η [24, 25]:

$$\omega = p_0 + p_1 \times (\eta - \langle\eta\rangle) \tag{5}$$

with $\langle\eta\rangle$ being the mean of the distribution of η. This parametrization is chosen to minimize the correlations between p_0 and p_1. The calibration is performed separately for the OST and SST.

The sets of calibration parameters $(p_0, p_1)_{\mathrm{OST}}$ and $(p_0, p_1)_{\mathrm{SST}}$ are allowed to vary in the fit. The figure of merit of these tagging algorithms is called the effective tagging efficiency $\varepsilon_{\mathrm{eff}}$. It gives the factor by which the statistical power of the sample is reduced due to imperfect tagging decisions. In this analysis, $\varepsilon_{\mathrm{eff}}$ is found to be $(2.6 \pm 0.4)\%$ for the OST and $(1.2 \pm 0.3)\%$ for the SST. Uncertainties are statistical only.

7. Measurement of Δm_s

Adding the information of the flavour tagging algorithms, the decay time PDF for tagged signal candidates is modified to

$$\mathcal{P}_t(t|\sigma_t) \propto \left\{ \Gamma_s \, \mathrm{e}^{-\Gamma_s t} \, \frac{1}{2} \left[\cosh\left(\frac{\Delta\Gamma_s}{2} t \right) + q \, [1 - 2\omega(\eta_{\mathrm{OST}}, \eta_{\mathrm{SST}})] \cos(\Delta m_s t) \right] \theta(t) \right\} \otimes G(t, S_{\sigma_t}\sigma_t) \, \mathcal{E}_t(t) \, \epsilon, \tag{6}$$

where ϵ gives the fraction of candidates with a tagging decision. Signal candidates without a tagging decision are still described by equation (4) multiplied by an additional factor $(1 - \epsilon)$ to ensure relative normalization.

The information provided by the opposite-side and same-side taggers for the signal is combined to a single tagging decision q and a single mistag probability $\omega(\eta_{\mathrm{OST}}, \eta_{\mathrm{SST}})$ using their respective calibration parameters $p_{0_{\mathrm{OST/SST}}}$ and $p_{1_{\mathrm{OST/SST}}}$. The individual background components show different tagging characteristics for candidates tagged by the OST or SST. The b hadron backgrounds show the same opposite-side tagging behaviour (q and ω) as the signal, while the combinatorial background shows random tagging behaviour. For same-side tagged events, we assume random tagging behaviour for all background components. We introduce tagging asymmetry parameters to allow for different numbers of candidates being tagged as mixed or unmixed, and other parameters to describe the tagging efficiencies for these backgrounds. As expected, the fitted values of these asymmetry parameters are consistent with zero within uncertainties.

All tagging parameters, as well as the value for Δm_s, are constrained to be the same for the five decay modes. The result is $\Delta m_s = 17.768 \pm 0.023\,\mathrm{ps}^{-1}$ (statistical uncertainty only). The likelihood profile was examined and found to have a Gaussian shape up to nine standard deviations. The decay time distributions for candidates tagged as mixed or unmixed are shown in figure 2, together with the decay time projections of the PDF distributions resulting from the fit.

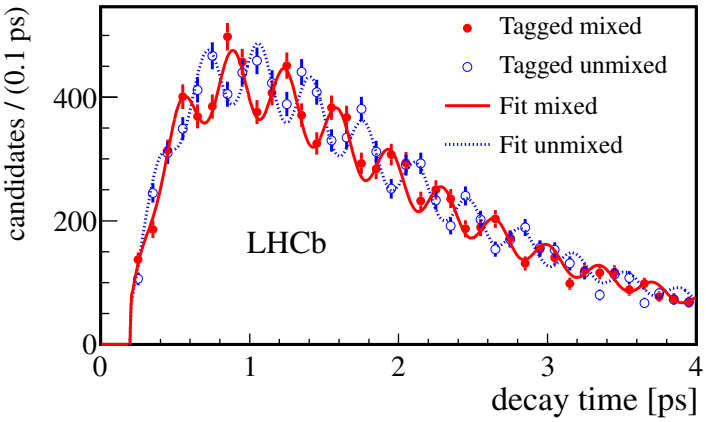

Figure 2. Decay time distribution for the sum of the five decay modes for candidates tagged as mixed (different flavour at decay and production; red, continuous line) or unmixed (same flavour at decay and production; blue, dotted line). The data and the fit projections are plotted in a signal window around the reconstructed B_s^0 mass of 5.32–5.55 GeV/c^2.

8. Systematic uncertainties

With respect to the first measurement of Δm_s at LHCb [13], all sources of systematic uncertainties have been reevaluated.

The dominant source is related to the knowledge of the absolute value of the decay time. This has two main contributions. First, the imperfect knowledge of the longitudinal (z) scale of the detector contributes to the systematic uncertainty. It is obtained by comparing the track-based alignment and survey data and evaluating the track distribution in the vertex detector. This results in 0.02% uncertainty on the decay time scale and thus an absolute uncertainty of $\pm 0.004\,\text{ps}^{-1}$ on Δm_s.

The second contribution to the uncertainty of the decay time scale comes from the knowledge of the overall momentum scale. This has been evaluated by an independent study using mass measurements of well-known resonances. Deviations from the reference values [27] are measured to be within 0.15%. However, since both the measured invariant mass and momentum enter the calculation of the decay time, this effect cancels to some extent. The resulting systematic uncertainty on the decay time scale is evaluated from simulation to be 0.02%. This again translates to an absolute uncertainty of $\pm 0.004\,\text{ps}^{-1}$ on Δm_s.

The next largest systematic uncertainty is due to a possible bias of the measured decay time given by the track reconstruction and the selection procedure. This is estimated from simulated data to be less than about 0.2 fs, and results in $\pm 0.001\,\text{ps}^{-1}$ systematic uncertainty on Δm_s.

Various other sources contributing to the systematic uncertainty have been studied such as the decay time acceptance, decay time resolution, variations of the value of $\Delta\Gamma_s$, different signal models for the invariant mass and the decay time resolution, variations of the signal fraction and the fraction of $B_s^0 \to D_s^{\mp} K^{\pm}$ candidates. They are all found to be negligible. The sources of systematic uncertainty on the measurement of Δm_s are summarized in table 2.

Table 2. Systematic uncertainties on the Δm_s measurement. The total systematic uncertainty is calculated as the quadratic sum of the individual contributions.

Source	Uncertainty (ps^{-1})
z-scale	0.004
Momentum scale	0.004
Decay time bias	0.001
Total systematic uncertainty	0.006

9. Conclusion

A measurement of the B_s^0– $\overline{B}_s^0$ oscillation frequency Δm_s is performed using $B_s^0 \to D_s^- \pi^+$ decays in five different D_s^- decay channels. Using a data sample corresponding to an integrated luminosity of $1.0\,fb^{-1}$ collected by LHCb in 2011, the oscillation frequency is found to be

$$\Delta m_s = 17.768 \pm 0.023\,(\text{stat}) \pm 0.006\,(\text{syst})\,ps^{-1},$$

in good agreement with the first result reported by the LHCb experiment [13] and the current world average, $17.69 \pm 0.08\,ps^{-1}$ [27]. This is the most precise measurement of Δm_s to date, and will be a crucial ingredient in future searches for BSM physics in B_s^0 oscillations.

Acknowledgments

We express our gratitude to our colleagues in the CERN accelerator departments for the excellent performance of the LHC. We thank the technical and administrative staff at the LHCb institutes. We acknowledge support from CERN and from the national agencies: CAPES, CNPq, FAPERJ and FINEP (Brazil); NSFC (China); CNRS/IN2P3 and Region Auvergne (France); BMBF, DFG, HGF and MPG (Germany); SFI (Ireland); INFN (Italy); FOM and NWO (The Netherlands); SCSR (Poland); ANCS/IFA (Romania); MinES, Rosatom, RFBR and NRC 'Kurchatov Institute' (Russia); MinECo, XuntaGal and GENCAT (Spain); SNSF and SER (Switzerland); NAS Ukraine (Ukraine); STFC (UK); and NSF (USA). We also acknowledge the support received from the ERC under FP7. The Tier1 computing centres are supported by IN2P3 (France), KIT and BMBF (Germany), INFN (Italy), NWO and SURF (The Netherlands), PIC (Spain) and GridPP (UK). We are thankful for the computing resources put at our disposal by Yandex LLC (Russia), as well as to the communities behind the multiple open source software packages that we depend on.

The LHCb Collaboration

R Aaij[40], C Abellan Beteta[35,73], B Adeva[36], M Adinolfi[45], C Adrover[6], A Affolder[51], Z Ajaltouni[5], J Albrecht[9], F Alessio[37], M Alexander[50], S Ali[40], G Alkhazov[29], P Alvarez Cartelle[36], A A Alves Jr[24,37], S Amato[2], S Amerio[21], Y Amhis[7], L Anderlini[17,65], J Anderson[39], R Andreassen[56], R B Appleby[53], O Aquines Gutierrez[10], F Archilli[18], A Artamonov[34], M Artuso[57], E Aslanides[6], G Auriemma[24,72], S Bachmann[11], J J Back[47], C Baesso[58], V Balagura[30], W Baldini[16], R J Barlow[53], C Barschel[37], S Barsuk[7], W Barter[46], Th Bauer[40], A Bay[38], J Beddow[50], F Bedeschi[22], I Bediaga[1], S Belogurov[30], K Belous[34], I Belyaev[30], E Ben-Haim[8], M Benayoun[8], G Bencivenni[18], S Benson[49], J Benton[45],

A Berezhnoy[31], R Bernet[39], M-O Bettler[46], M van Beuzekom[40], A Bien[11], S Bifani[44], T Bird[53], A Bizzeti[17,67], P M Bjørnstad[53], T Blake[37], F Blanc[38], J Blouw[11], S Blusk[57], V Bocci[24], A Bondar[33], N Bondar[29], W Bonivento[15], S Borghi[53], A Borgia[57], T J V Bowcock[51], E Bowen[39], C Bozzi[16], T Brambach[9], J van den Brand[41], J Bressieux[38], D Brett[53], M Britsch[10], T Britton[57], N H Brook[45], H Brown[51], I Burducea[28], A Bursche[39], G Busetto[21,76], J Buytaert[37], S Cadeddu[15], O Callot[7], M Calvi[20,69], M Calvo Gomez[35,73], A Camboni[35], P Campana[18,37], D Campora Perez[37], A Carbone[14,62], G Carboni[23,70], R Cardinale[19,68], A Cardini[15], H Carranza-Mejia[49], L Carson[52], K Carvalho Akiba[2], G Casse[51], M Cattaneo[37], Ch Cauet[9], M Charles[54], Ph Charpentier[37], P Chen[3,38], N Chiapolini[39], M Chrzaszcz[25], K Ciba[37], X Cid Vidal[37], G Ciezarek[52], P E L Clarke[49], M Clemencic[37], H V Cliff[46], J Closier[37], C Coca[28], V Coco[40], J Cogan[6], E Cogneras[5], P Collins[37], A Comerma-Montells[35], A Contu[15,37], A Cook[45], M Coombes[45], S Coquereau[8], G Corti[37], B Couturier[37], G A Cowan[49], D C Craik[47], S Cunliffe[52], R Currie[49], C D'Ambrosio[37], P David[8], P N Y David[40], I De Bonis[4], K De Bruyn[40], S De Capua[53], M De Cian[39], J M De Miranda[1], L De Paula[2], W De Silva[56], P De Simone[18], D Decamp[4], M Deckenhoff[9], L Del Buono[8], D Derkach[14], O Deschamps[5], F Dettori[41], A Di Canto[11], H Dijkstra[37], M Dogaru[28], S Donleavy[51], F Dordei[11], A Dosil Suárez[36], D Dossett[47], A Dovbnya[42], F Dupertuis[38], R Dzhelyadin[34], A Dziurda[25], A Dzyuba[29], S Easo[48,37], U Egede[52], V Egorychev[30], S Eidelman[33], D van Eijk[40], S Eisenhardt[49], U Eitschberger[9], R Ekelhof[9], L Eklund[50,37], I El Rifai[5], Ch Elsasser[39], D Elsby[44], A Falabella[14,64], C Färber[11], G Fardell[49], C Farinelli[40], S Farry[12], V Fave[38], D Ferguson[49], V Fernandez Albor[36], F Ferreira Rodrigues[1], M Ferro-Luzzi[37], S Filippov[32], M Fiore[16], C Fitzpatrick[37], M Fontana[10], F Fontanelli[19,68], R Forty[37], O Francisco[2], M Frank[37], C Frei[37], M Frosini[17,65], S Furcas[20], E Furfaro[23,70], A Gallas Torreira[36], D Galli[14,62], M Gandelman[2], P Gandini[57], Y Gao[3], J Garofoli[57], P Garosi[53], J Garra Tico[46], L Garrido[35], C Gaspar[37], R Gauld[54], E Gersabeck[11], M Gersabeck[53], T Gershon[47,37], Ph Ghez[4], V Gibson[46], V V Gligorov[37], C Göbel[58], D Golubkov[30], A Golutvin[52,30,37], A Gomes[2], H Gordon[54], M Grabalosa Gándara[5], R Graciani Diaz[35], L A Granado Cardoso[37], E Graugés[35], G Graziani[17], A Grecu[28], E Greening[54], S Gregson[46], O Grünberg[59], B Gui[57], E Gushchin[32], Yu Guz[34,37], T Gys[37], C Hadjivasiliou[57], G Haefeli[38], C Haen[37], S C Haines[46], S Hall[52], T Hampson[45], S Hansmann-Menzemer[11], N Harnew[54], S T Harnew[45], J Harrison[53], T Hartmann[59], J He[37], V Heijne[40], K Hennessy[51], P Henrard[5], J A Hernando Morata[36], E van Herwijnen[37], E Hicks[51], D Hill[54], M Hoballah[5], C Hombach[53], P Hopchev[4], W Hulsbergen[40], P Hunt[54], T Huse[51], N Hussain[54], D Hutchcroft[51], D Hynds[50], V Iakovenko[43], M Idzik[26], P Ilten[12], R Jacobsson[37], A Jaeger[11], E Jans[40], P Jaton[38], F Jing[3], M John[54], D Johnson[54], C R Jones[46], B Jost[37], M Kaballo[9], S Kandybei[42], M Karacson[37], T M Karbach[37], I R Kenyon[44], U Kerzel[37], T Ketel[41], A Keune[38], B Khanji[20], O Kochebina[7], I Komarov[38], R F Koopman[41], P Koppenburg[40], M Korolev[31], A Kozlinskiy[40], L Kravchuk[32], K Kreplin[11], M Kreps[47], G Krocker[11], P Krokovny[33], F Kruse[9], M Kucharczyk[20,25,69], V Kudryavtsev[33], T Kvaratskheliya[30,37], V N La Thi[38], D Lacarrere[37], G Lafferty[53], A Lai[15], D Lambert[49], R W Lambert[41], E Lanciotti[37], G Lanfranchi[18], C Langenbruch[37], T Latham[47], C Lazzeroni[44], R Le Gac[6], J van Leerdam[40], J-P Lees[4], R Lefèvre[5], A Leflat[31], J Lefrançois[7], S Leo[22], O Leroy[6], T Lesiak[25], B Leverington[11], Y Li[3], L Li Gioi[5], M Liles[51], R Lindner[37], C Linn[11], B Liu[3], G Liu[37], S Lohn[37], I Longstaff[50], J H Lopes[2], E Lopez Asamar[35], N Lopez-March[38], H Lu[3], D Lucchesi[21,76], J Luisier[38], H Luo[49], F Machefert[7], I V Machikhiliyan[4,30], F Maciuc[28], O Maev[29,37], S Malde[54], G Manca[15,63], G Mancinelli[6], U Marconi[14], R Märki[38], J Marks[11], G Martellotti[24], A Martens[8], L Martin[54], A Martín Sánchez[7], M Martinelli[40], D Martinez Santos[41], D Martins Tostes[2],

A Massafferri[1], R Matev[37], Z Mathe[37], C Matteuzzi[20], E Maurice[6], A Mazurov[16,32,37,64], J McCarthy[44], A McNab[53], R McNulty[12], B Meadows[56,54], F Meier[9], M Meissner[11], M Merk[40], D A Milanes[8], M-N Minard[4], J Molina Rodriguez[58], S Monteil[5], D Moran[53], P Morawski[25], M J Morello[22,78], R Mountain[57], I Mous[40], F Muheim[49], K Müller[39], R Muresan[28], B Muryn[26], B Muster[38], P Naik[45], T Nakada[38], R Nandakumar[48], I Nasteva[1], M Needham[49], N Neufeld[37], A D Nguyen[38], T D Nguyen[38], C Nguyen-Mau[38,75], M Nicol[7], V Niess[5], R Niet[9], N Nikitin[31], T Nikodem[11], A Nomerotski[54], A Novoselov[34], A Oblakowska-Mucha[26], V Obraztsov[34], S Oggero[40], S Ogilvy[50], O Okhrimenko[43], R Oldeman[15,63], M Orlandea[28], J M Otalora Goicochea[2], P Owen[52], A Oyanguren [35,74], B K Pal[57], A Palano[13,61], M Palutan[18], J Panman[37], A Papanestis[48], M Pappagallo[50], C Parkes[53], C J Parkinson[52], G Passaleva[17], G D Patel[51], M Patel[52], G N Patrick[48], C Patrignani[19,68], C Pavel-Nicorescu[28], A Pazos Alvarez[36], A Pellegrino[40], G Penso[24,71], M Pepe Altarelli[37], S Perazzini[14,62], D L Perego[20,69], E Perez Trigo[36], A Pérez-Calero Yzquierdo[35], P Perret[5], M Perrin-Terrin[6], G Pessina[20], K Petridis[52], A Petrolini[19,68], A Phan[57], E Picatoste Olloqui[35], B Pietrzyk[4], T Pilař[47], D Pinci[24], S Playfer[49], M Plo Casasus[36], F Polci[8], G Polok[25], A Poluektov[47,33], E Polycarpo[2], D Popov[10], B Popovici[28], C Potterat[35], A Powell[54], J Prisciandaro[38], V Pugatch[43], A Puig Navarro[38], G Punzi[22,77], W Qian[4], J H Rademacker[45], B Rakotomiaramanana[38], M S Rangel[2], I Raniuk[42], N Rauschmayr[37], G Raven[41], S Redford[54], M M Reid[47], A C dos Reis[1], S Ricciardi[48], A Richards[52], K Rinnert[51], V Rives Molina[35], D A Roa Romero[5], P Robbe[7], E Rodrigues[53], P Rodriguez Perez[36], S Roiser[37], V Romanovsky[34], A Romero Vidal[36], J Rouvinet[38], T Ruf[37], F Ruffini[22], H Ruiz[35], P Ruiz Valls[35,74], G Sabatino[24,70], J J Saborido Silva[36], N Sagidova[29], P Sail[50], B Saitta[15,63], C Salzmann[39], B Sanmartin Sedes[36], M Sannino[19,68], R Santacesaria[24], C Santamarina Rios[36], E Santovetti[23,70], M Sapunov[6], A Sarti[18,71], C Satriano[24,72], A Satta[23], M Savrie[16,64], D Savrina[30,31], P Schaack[52], M Schiller[41], H Schindler[37], M Schlupp[9], M Schmelling[10], B Schmidt[37], O Schneider[38], A Schopper[37], M-H Schune[7], R Schwemmer[37], B Sciascia[18], A Sciubba[24], M Seco[36], A Semennikov[30], K Senderowska[26], I Sepp[52], N Serra[39], J Serrano[6], P Seyfert[11], M Shapkin[34], I Shapoval[16,42], P Shatalov[30], Y Shcheglov[29], T Shears[51,37], L Shekhtman[33], O Shevchenko[42], V Shevchenko[30], A Shires[52], R Silva Coutinho[47], T Skwarnicki[57], N A Smith[51], E Smith[54,48], M Smith[53], M D Sokoloff[56], F J P Soler[50], F Soomro[18], D Souza[45], B Souza De Paula[2], B Spaan[9], A Sparkes[49], P Spradlin[50], F Stagni[37], S Stahl[11], O Steinkamp[39], S Stoica[28], S Stone[57], B Storaci[39], M Straticiuc[28], U Straumann[39], V K Subbiah[37], S Swientek[9], V Syropoulos[41], M Szczekowski[27], P Szczypka[38,37], T Szumlak[26], S T'Jampens[4], M Teklishyn[7], E Teodorescu[28], F Teubert[37], C Thomas[54], E Thomas[37], J van Tilburg[11], V Tisserand[4], M Tobin[38], S Tolk[41], D Tonelli[37], S Topp-Joergensen[54], N Torr[54], E Tournefier[4,52], S Tourneur[38], M T Tran[38], M Tresch[39], A Tsaregorodtsev[6], P Tsopelas[40], N Tuning[40], M Ubeda Garcia[37], A Ukleja[27], D Urner[53], U Uwer[11], V Vagnoni[14], G Valenti[14], R Vazquez Gomez[35], P Vazquez Regueiro[36], S Vecchi[16], J J Velthuis[45], M Veltri[17,66], G Veneziano[38], M Vesterinen[37], B Viaud[7], D Vieira[2], X Vilasis-Cardona[35,73], A Vollhardt[39], D Volyanskyy[10], D Voong[45], A Vorobyev[29], V Vorobyev[33], C Voß[59], H Voss[10], R Waldi[59], R Wallace[12], S Wandernoth[11,79], J Wang[57], D R Ward[46], N K Watson[44], A D Webber[53], D Websdale[52], M Whitehead[47], J Wicht[37], J Wiechczynski[25], D Wiedner[11], L Wiggers[40], G Wilkinson[54], M P Williams[47,48], M Williams[55], F F Wilson[48], J Wishahi[9], M Witek[25], S A Wotton[46], S Wright[46], S Wu[3], K Wyllie[37], Y Xie[49,37], F Xing[54], Z Xing[57], Z Yang[3], R Young[49], X Yuan[3], O Yushchenko[34], M Zangoli[14], M Zavertyaev[10,60], F Zhang[3], L Zhang[57], W C Zhang[12], Y Zhang[3], A Zhelezov[11], A Zhokhov[30], L Zhong[3] and A Zvyagin[37]

[1] Centro Brasileiro de Pesquisas Físicas (CBPF), Rio de Janeiro, Brazil
[2] Universidade Federal do Rio de Janeiro (UFRJ), Rio de Janeiro, Brazil
[3] Center for High Energy Physics, Tsinghua University, Beijing, People's Republic of China
[4] LAPP, Université de Savoie, CNRS/IN2P3, Annecy-Le-Vieux, France
[5] Clermont Université, Université Blaise Pascal, CNRS/IN2P3, LPC, Clermont-Ferrand, France
[6] CPPM, Aix-Marseille Université, CNRS/IN2P3, Marseille, France
[7] LAL, Université Paris-Sud, CNRS/IN2P3, Orsay, France
[8] LPNHE, Université Pierre et Marie Curie, Université Paris Diderot, CNRS/IN2P3, Paris, France
[9] Fakultät Physik, Technische Universität Dortmund, Dortmund, Germany
[10] Max-Planck-Institut für Kernphysik (MPIK), Heidelberg, Germany
[11] Physikalisches Institut, Ruprecht-Karls-Universität Heidelberg, Heidelberg, Germany
[12] School of Physics, University College Dublin, Dublin, Ireland
[13] Sezione INFN di Bari, Bari, Italy
[14] Sezione INFN di Bologna, Bologna, Italy
[15] Sezione INFN di Cagliari, Cagliari, Italy
[16] Sezione INFN di Ferrara, Ferrara, Italy
[17] Sezione INFN di Firenze, Firenze, Italy
[18] Laboratori Nazionali dell'INFN di Frascati, Frascati, Italy
[19] Sezione INFN di Genova, Genova, Italy
[20] Sezione INFN di Milano Bicocca, Milano, Italy
[21] Sezione INFN di Padova, Padova, Italy
[22] Sezione INFN di Pisa, Pisa, Italy
[23] Sezione INFN di Roma Tor Vergata, Roma, Italy
[24] Sezione INFN di Roma La Sapienza, Roma, Italy
[25] Henryk Niewodniczanski Institute of Nuclear Physics Polish Academy of Sciences, Kraków, Poland
[26] AGH—University of Science and Technology, Faculty of Physics and Applied Computer Science, Kraków, Poland
[27] National Center for Nuclear Research (NCBJ), Warsaw, Poland
[28] Horia Hulubei National Institute of Physics and Nuclear Engineering, Bucharest-Magurele, Romania
[29] Petersburg Nuclear Physics Institute (PNPI), Gatchina, Russia
[30] Institute of Theoretical and Experimental Physics (ITEP), Moscow, Russia
[31] Institute of Nuclear Physics, Moscow State University (SINP MSU), Moscow, Russia
[32] Institute for Nuclear Research of the Russian Academy of Sciences (INR RAN), Moscow, Russia
[33] Budker Institute of Nuclear Physics (SB RAS) and Novosibirsk State University, Novosibirsk, Russia
[34] Institute for High Energy Physics (IHEP), Protvino, Russia
[35] Universitat de Barcelona, Barcelona, Spain
[36] Universidad de Santiago de Compostela, Santiago de Compostela, Spain
[37] European Organization for Nuclear Research (CERN), Geneva, Switzerland
[38] Ecole Polytechnique Fédérale de Lausanne (EPFL), Lausanne, Switzerland
[39] Physik-Institut, Universität Zürich, Zürich, Switzerland
[40] Nikhef National Institute for Subatomic Physics, Amsterdam, The Netherlands

[41] Nikhef National Institute for Subatomic Physics and VU University Amsterdam, Amsterdam, The Netherlands
[42] NSC Kharkiv Institute of Physics and Technology (NSC KIPT), Kharkiv, Ukraine
[43] Institute for Nuclear Research of the National Academy of Sciences (KINR), Kyiv, Ukraine
[44] University of Birmingham, Birmingham, UK
[45] H H Wills Physics Laboratory, University of Bristol, Bristol, UK
[46] Cavendish Laboratory, University of Cambridge, Cambridge, UK
[47] Department of Physics, University of Warwick, Coventry, UK
[48] STFC Rutherford Appleton Laboratory, Didcot, UK
[49] School of Physics and Astronomy, University of Edinburgh, Edinburgh, UK
[50] School of Physics and Astronomy, University of Glasgow, Glasgow, UK
[51] Oliver Lodge Laboratory, University of Liverpool, Liverpool, UK
[52] Imperial College London, London, UK
[53] School of Physics and Astronomy, University of Manchester, Manchester, UK
[54] Department of Physics, University of Oxford, Oxford, UK
[55] Massachusetts Institute of Technology, Cambridge, MA, USA
[56] University of Cincinnati, Cincinnati, OH, USA
[57] Syracuse University, Syracuse, NY, USA
[58] Pontifícia Universidade Católica do Rio de Janeiro (PUC-Rio), Rio de Janeiro, Brazil, associated to Universidade Federal do Rio de Janeiro (UFRJ), Rio de Janeiro, Brazil
[59] Institut für Physik, Universität Rostock, Rostock, Germany, associated to Physikalisches Institut, Ruprecht-Karls-Universität Heidelberg, Heidelberg, Germany
[60] P N Lebedev Physical Institute, Russian Academy of Science (LPI RAS), Moscow, Russia
[61] Università di Bari, Bari, Italy
[62] Università di Bologna, Bologna, Italy
[63] Università di Cagliari, Cagliari, Italy
[64] Università di Ferrara, Ferrara, Italy
[65] Università di Firenze, Firenze, Italy
[66] Università di Urbino, Urbino, Italy
[67] Università di Modena e Reggio Emilia, Modena, Italy
[68] Università di Genova, Genova, Italy
[69] Università di Milano Bicocca, Milano, Italy
[70] Università di Roma Tor Vergata, Roma, Italy
[71] Università di Roma La Sapienza, Roma, Italy
[72] Università della Basilicata, Potenza, Italy
[73] LIFAELS, La Salle, Universitat Ramon Llull, Barcelona, Spain
[74] IFIC, Universitat de Valencia-CSIC, Valencia, Spain
[75] Hanoi University of Science, Hanoi, Vietnam
[76] Università di Padova, Padova, Italy
[77] Università di Pisa, Pisa, Italy
[78] Scuola Normale Superiore, Pisa, Italy
[79] Author to whom any correspondence should be addressed.

References

[1] Adeva B *et al* (LHCb Collaboration) 2009 Roadmap for selected key measurements of LHCb arXiv:0912.4179

[2] Aaij R *et al* (LHCb Collaboration) 2013 Implications of LHCb measurements and future prospects *Eur. Phys. J.* C **73** 2373
[3] Lande K *et al* 1956 Observation of long-lived neutral V, particles *Phys. Rev.* **103** 1901
[4] Albrecht H *et al* (ARGUS Collaboration) 1987 Observation of B^0–anti-B^0 mixing *Phys. Lett.* B **192** 245
[5] Abazov V *et al* (D0 Collaboration) 2006 First direct two-sided bound on the B_s^0 oscillation frequency *Phys. Rev. Lett.* **97** 021802
[6] Abulencia A *et al* (CDF Collaboration) 2006 Observation of B_s^0–anti-B_s^0 oscillations *Phys. Rev. Lett.* **97** 242003
[7] Aubert B *et al* (BaBar Collaboration) 2009 Measurement of D^0–$\overline{D}^0$ mixing from a, time-dependent amplitude analysis of $D^0 \to K^+\pi^-\pi^0$ decays *Phys. Rev. Lett.* **103** 211801
[8] Staric M *et al* (Belle Collaboration) 2007 Evidence for D^0–$\overline{D}^0$ mixing *Phys. Rev. Lett.* **98** 211803
[9] Aaltonen T *et al* (CDF Collaboration) 2008 Evidence for D^0–$\overline{D}^0$ mixing using the CDF II detector *Phys. Rev. Lett.* **100** 121802
[10] Aaij R *et al* (LHCb Collaboration) 2013 Observation of D^0–$\overline{D}^0$ oscillations *Phys. Rev. Lett.* **110** 101802
[11] Lenz A and Nierste U 2007 Theoretical update of B_s–$\overline{B}_s$ mixing *J. High Energy Phys.* JHEP06(2007)072
[12] Aaij R *et al* (LHCb Collaboration) 2013 Measurement of CP violation and the B_s^0 meson decay width difference with $B_s^0 \to J/\psi K^+K^-$ and $B_s^0 \to J/\psi\pi^+\pi^-$ decays *Phys. Rev.* D submitted (arXiv:1304.2600)
[13] Aaij R *et al* (LHCb Collaboration) 2012 Measurement of the B_s^0–$\overline{B}_s^0$ oscillation frequency Δm_s in $B_s^0 \to D_s^-(3)\pi$ decays *Phys. Lett.* B **709** 177
[14] Alves A A Jr *et al* (LHCb Collaboration) 2008 The LHCb detector at the LHC *J. Instrum.* **3** S08005
[15] Adinolfi M *et al* 2012 Performance of the LHCb RICH detector at the LHC *Eur. Phys. J.* C submitted (arXiv:1211.6759)
[16] Aaij R *et al* 2013 The LHCb trigger and its performance in 2011 *J. Instrum.* **8** P04022
[17] Sjöstrand T, Mrenna S and Skands P 2006 PYTHIA 64 physics and manual *J. High Energy Phys.* JHEP05(2006)026
[18] Belyaev I *et al* 2010 Handling of the generation of primary events in GAUSS the LHCb simulation framework *Nuclear Science Symp. Conf. Record (NSS/MIC)* (Piscataway, NJ: IEEE) p 1155
[19] Lange D J 2001 The EvtGen particle decay simulation package *Nucl. Instrum. Methods* A **462** 152
[20] Golonka P and Was Z 2006 PHOTOS Monte Carlo: a, precision tool for QED corrections in Z and W decays *Eur. Phys. J.* C **45** 97
[21] Allison J *et al* (GEANT4 Collaboration) 2006 Geant4 developments and applications *IEEE Trans. Nucl. Sci.* **53** 270
[22] Agostinelli S *et al* (GEANT4 Collaboration) 2003 GEANT4: a, simulation toolkit *Nucl. Instrum. Meth.* A **506** 250
[23] Clemencic M *et al* 2011 The LHCb simulation application GAUSS: design evolution and experience *J. Phys.: Conf. Ser.* **331** 032023
[24] Aaij R *et al* (LHCb Collaboration) 2012 Opposite-side flavour tagging of B mesons at the LHCb experiment *Eur. Phys. J.* C **72** 2022
[25] LHCb Collaboration 2012 Optimization and calibration of the same-side kaon tagging algorithm using hadronic B_s^0 decays in 2011 data LHCb-CONF-2012-033
[26] Breiman L, Friedman J H, Olshen R A and Stone C J 1984 *Classification and Regression Trees* (Belmont, CA: Wadsworth International Group)
[27] Beringer J *et al* 2012 (Particle Data Group) Review of particle physics *Phys. Rev.* D **86** 010001
[28] Punzi G 2003 Comments on likelihood fits with variable resolution eConf C030908 WELT002
[29] Skwarnicki T 1986 A study of the radiative cascade transitions between the upsilon-prime and upsilon resonances *PhD Thesis* Institute of Nuclear Physics Krakow DESY-F31-86-02 (http://inspirehep.net/record/230779/files/230779.pdf)